Lattice instabilities and ferroelectricity in AScO$_3$ perovskite alloys

S. V. Halilov,[1,2] M. Fornari,[3] and D. J. Singh[1]
[1]*Center for Computational Materials Science, Naval Research Laboratory, Washington, DC 20375, USA*
[2]*Department of Materials Science and Engineering, University of Pennsylvania, Philadelphia, Pennsylvania 19104, USA*
[3]*Department of Physics, Central Michigan University, Mt. Pleasant, Michigan 48859, USA*
(Received 29 January 2004; published 21 May 2004)

The structural properties and lattice instabilities of perovskites in the (Th,Pb,Bi,Y)ScO$_3$ system are investigated by first-principles density-functional calculations with the linearized augmented plane-wave method. In all cases, Th is found to be tetravalent on the perovskite A site. The electronic structures have substantial Sc-O hybridization, as well as both Pb-O covalency, as is common in Pb based transition-metal perovskites, and significant hybridization of nominally unoccupied Th p and d states with O p states. The calculations show that the ideal cubic perovskite structure is highly unstable in (Th,Pb)ScO$_3$. The dominant instability is against rotation of the ScO$_6$ octahedra, as is common in perovskites with small A-site cations as defined by the perovskite tolerance factor. However, there are also substantial, though weaker, instabilities against ferroelectric distortions. These are characterized by large shifts of the A-site ions against the surrounding O, especially for the Th. The tetragonal ferroelectric state is favored over a rhombohedral state, and in addition a large tetragonal c/a ratio is found. At least for a particular ordering of the A-site ions we find that the ferroelectric and rotational distortions coexist, yielding a monoclinic symmetry ferroelectric ground state with rotated octahedra and a large Th off-centering. Calculations are also reported for BiScO$_3$ and YScO$_3$ in the perovskite structure. Considering only ferroelectric instabilities, these compounds show somewhat different anisotropies but both favor large c/a ratios when tetragonal. The instability against rotation of the ScO$_6$ octahedra is similar in energy to the ferroelectric instability in BiScO$_3$ and substantially stronger than the ferroelectric instability in YScO$_3$. Trends in the lattice instabilities of AScO$_3$ perovskites are discussed in terms of these results. Of the systems considered, the most likely to show a piezoelectrically active morphotropic phase boundary is Th$_{(1-x)/2}$Bi$_x$Pb$_{(1-x)/2}$ScO$_3$. Implications for practical piezoelectric materials are discussed.

DOI: 10.1103/PhysRevB.69.174107 PACS number(s): 77.84.Dy, 71.20.Ps

I. INTRODUCTION

Ferroelectric perovskite oxides ABO$_3$ play important roles in key technologies, including ferroelectric memories, tunable dielectric components (e.g., for antennae and microwave applications), and piezoelectric transducers (e.g., for medical ultrasound).[1–3] As was elucidated early on,[4,5] ferroelectricity in perovskites depends on delicate interplays of different competing interactions, particularly a balance of large interactions—long-range Coulomb interactions vs closed-shell ionic interactions, with the balance tipped by smaller effects related to covalency between metal ions and O p states.

The situation is even more complex in piezoelectrics, where the piezoelectric performance depends on the presence of a morphotropic phase boundary (MPB) between rhombohedral (pseudocubic) and tetragonal ferroelectric states in alloy phase diagrams, i.e., on the balance between different competing ferroelectric instabilities.[2,3,6–11] In particular, the piezoelectric performance in these materials originates in a polarization rotation from the rhombohedral towards the tetragonal phase, close to the MPB. There is presently considerable theoretical and experimental effort aimed at microscopic understanding of the underlying physics that determines the performance of these materials, and finding better compositions for applications.[12] Much of the current work emphasizes Pb based pseudobinaries with PbTiO$_3$, in particular PbBO$_3$-PbTiO$_3$, where B is four-valent metal, or mixture, e.g., $B=$Zr, Mg$_{1/3}$Nb$_{2/3}$, Zn$_{1/3}$Nb$_{2/3}$, although there is increasing interest in alternatives such as materials containing (Na,Bi)TiO$_3$ and the BiScO$_3$-PbTiO$_3$ alloy system.[13–15] Several reports[16–19] of supercell calculations have been made for intermediate compositions in the PZT system, mainly focusing on the B-site alloying.

The piezoelectric perovskite ferroelectrics, including Pb(Zr,Ti)O$_3$ (PZT) alloys, which are the basis of most current transducers, have so-called A-site driven ferroelectricity. This means that the ferroelectric distortions of the cubic perovskite lattice are mainly described as a shift of the A-site cation with respect to the surrounding oxygen ions with smaller accompanying shifts of the B-site ions. In these materials, the perovskite tolerance factor, $t=(r_A+r_O)/\sqrt{2}(r_B+r_O)$ where r_A, r_B, and r_O are the ionic radii of the A, B, and O ions, respectively, is smaller than unity, indicating a tendency towards instabilities changing the A site–O distances.[20]

In almost all cases, perovskites with $t\ll 1$ have ground-state structures involving rotations of the BO$_6$ octahedra about various axes.[21] These structures preserve inversion symmetry and are not ferroelectric, as in, for example, CaTiO$_3$ or GdFeO$_3$. The A-site driven ferroelectrics are unusual; this unusual ferroelectric property has long been rationalized as a result of the polarizable lone pair in the 6s state of Pb^{2+} and Bi^{3+} and in fact first-principles calculations, which reproduce quantitatively the ferroelectric ground states of these materials, do show structure dependent hybridization involving the A-site ions.

This understanding has led to a common view that piezoelectric perovskites should have either Pb or Bi on the *A* site. In fact, little is actually known at the microscopic level about the trends in the lattice instabilities of *A*-site driven ferroelectric perovskites when alloyed with *A*-site ions other than Pb or Bi. However, recently, first-principles calculations for $CdTiO_3$-$PbTiO_3$ (Ref. 22) and $AgNbO_3$-$PbTiO_3$ (Ref. 23) supercells were reported. These suggested possibly favorable changes in properties related to piezoelectricity relative to pure PZT. For $CdTiO_3$ alloying with $PbTiO_3$ an increase in the tetragonal c/a ratio was predicted, which would be favorable for the maximum actuation at the MPB. Recent experiments support this prediction, but the solubility of $CdTiO_3$ in $PbTiO_3$ is too low to reach the MPB without additional alloying.[24]

Clearly, it is desirable to obtain a better microscopic understanding of the trends in the lattice instabilities of these perovskites with *A*-site substitutions. Here we report first-principles density-functional calculations of the electronic structure and lattice instabilities of simple perovskite supercells in the $(Th,Bi,Y,Pb)ScO_3$ system and discuss the trends found in the lattice instabilities. Th was selected because of the possibility that it would enter the perovskite *A* site as Th^{4+}, which would make it perhaps the only tetravalent ion other than perhaps U to enter this site with a $3d$ transition element *B*-site ion. We note that UNb_4O_{12} and $ThNb_4O_{12}$ are known perovskite compounds in which U^{4+} or Th^{4+} share the *A* site with vacancies.[25] The trivalent Sc ion was selected for the *B* site in part because its larger ionic radius (relative to Ti) and lower valence might be more conducive to the formation of Th *A*-site perovskites and because relatively little first-principles work has been done on scandates, even though they may be quite promising as piezoelectrics. In particular, high Curie temperature T_C at the MPB is desirable for piezoelectric applications. Among materials in common use, PZT has the highest MPB value of $T_C=386\,°C$, but in fact recent studies have shown that the MPB value of $T_C=450\,°C$ in $BiScO_3$-$PbTiO_3$ is superior,[13,14] while the piezoelectric coefficients in bulk,[14] or (001) epitaxial films,[26] are comparable to those of commercial PZT. First-principles studies of prospective end-point perovskite scandates, such as $YScO_3$ are of particular importance to understand the trends in microscopic terms, since these end points do not generally occur in the perovskite structure in nature. The average tolerance factor for $(Th,Pb)ScO_3$ is similar to $BiScO_3$, and so one may anticipate that like $BiScO_3$ it is on the borderline of perovskite stability.

II. METHOD

As mentioned, calculations were done for simple ordered supercells using density-functional theory within the standard local-density approximation (LDA). For this purpose, we used the general potential linearized augmented planewave (LAPW) method,[27] with local orbital extensions[28] to relax linearization errors and to treat the higher lying semicore states of the metal ions.

Convergence parameters were chosen as in our recent work on the $(Cd,Pb)TiO_3$ system.[22] LAPW sphere radii of $1.9a_0$, $2.0a_0$, $1.8a_0$, and $1.4a_0$ were used for Pb, Th, Sc, and O, respectively. The core states were treated fully relativistically, while valence states were treated within a scalar relativistic approximation. Valence spin-orbit effects are known to be important in obtaining accurate structural parameters for Th metal.[29,30] However, in the perovskites we are considering here, Th occurs as a four-valent ion, which might be expected to make valence spin-orbit effects less important. We checked this by doing some calculations of total-energy differences, both without spin orbit, and with spin orbit treated in a second variational approach as in Ref. 29. We found that the energy differences, including the energy of a ferroelectric structure relative to the ideal cubic perovskite, were not significantly affected by the inclusion of spin orbit on the valence states. Except as noted, all internal atomic positions are relaxed within the given symmetry of the cell. Also, unless otherwise noted, all calculations were done at the predicted LDA volumes. It should be noted that these are typically a few percent smaller than the experimental volumes in oxides. However, since the materials considered here have not been synthesized experimentally, a theoretical volume must be used. The calculated LDA lattice parameters for cubic perovskite $BiScO_3$ and $YScO_3$ are $7.54a_0$ and $7.40a_0$, respectively. The calculations for $Th_{0.5}Pb_{0.5}ScO_3$ were done with a 10 atom perovskite supercell, using a NaCl ordering of the *A*-site ions. The calculated effective lattice parameter of this cell is $7.55a_0$ (the fcc lattice parameter of the supercell was $15.10a_0$), which is very similar to that of $BiScO_3$. This may be an indication that solid solutions of $Th_{0.5}Pb_{0.5}ScO_3$ and $BiScO_3$ can be made in a substantial composition range, though the low tolerance factor, which indicates borderline perovskite stability, is a potential complication.

Unlike $Pb(Zr,Ti)O_3$, where strong volume dependencies affect the ground state,[18] one may expect the relatively soft ScO_6 octahedra in the present systems to give weaker volume dependencies, more analogous to those found in Sr_2RuO_4.[31] Some calculations were done at different volumes to test this, and in fact only weak volume dependence of the nonferroelectric lattice instabilities was found (see below). Calculations as a function of the tetragonal c/a ratio were performed at constant volume.

III. ELECTRONIC STRUCTURE

Calculated projections of the electronic density of states (DOS) for a 10 atom perovskite supercell of composition $ThPbSc_2O_6$ are shown in Fig. 1. As mentioned, this supercell is constructed by decorating the cubic perovskite *A*-site lattice with alternating Th and Pb atoms along all three Cartesian directions. Figure 1 also shows the DOS for a relaxed tetragonal ferroelectric state with $c/a=1.08$ and the projected DOS after a relaxation of this cell, keeping the lattice vectors the same, and fully optimizing the positions of the atoms within a monoclinic C_m space group. The relaxed structure has an energy 88 mRy below the ideal cubic structure on a per Sc basis and shortened *A* site–O bond lengths corresponding to a combination of rotation of the O octahedra and ferroelectric off-centerings of the ions.

The band structure in both the ideal cubic and relaxed

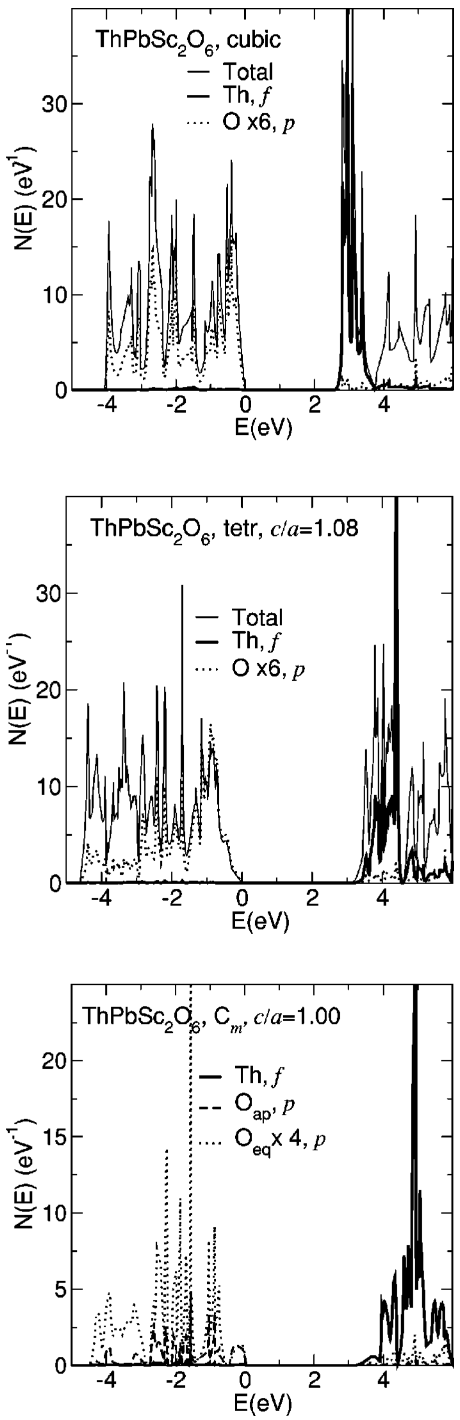

FIG. 1. Electronic density of states and projections for $ThPbSc_2O_6$ supercells (see text). The top panel shows the total density of states for the ideal cubic perovskite structure along with projections of Th f and O p character. The middle panel is for the relaxed tetragonal ferroelectric state with $c/a = 1.08$. The bottom shows the projections for a fully relaxed structure (space group C_m), keeping pseudocubic lattice vectors. O_{ap} and O_{eq} denotes the O closest to Th at the apex of the octahedra and O_{eq} denotes the O along the equator, with the apex and equator defined with respect to the main rotation axis. Note the increase in band gap upon structural relaxation. The projections are onto the LAPW spheres.

structures shows a gap between O $2p$ derived bands and unoccupied Th $5f$ derived bands. The higher lying conduction bands consist of mixed metal character, primarily Th d, Pb p, and Sc d derived. These overlap more strongly with the Th $5f$ states in the relaxed structure, since the Sc d and Th f move in opposite directions with the lattice distortions (note the $1s$ core-level positions, discussed below). The LDA band gaps are 2.6, 3.1, and 3.2 eV for the ideal cubic, the tetragonal ferroelectric, and the monoclinic relaxed structures, respectively. These may be underestimates as is common in density-functional calculations. As conjectured, Th is fourvalent in this compound, independent of structure.

As mentioned, covalency plays an important role in producing ferroelectric instabilities in perovskites and in distinguishing between different possible ferroelectric ground states. This has been discussed previously in the context of ferroelectrics with Pb and Bi A-site ions, both from the band structure[5] and from the crystal chemistry points of view, where the discussion is in terms of polarizable lone pairs of Pb and Bi. There is very little Th $5f$ character in the valence bands. However, the nominally O p derived valence bands do contain significant character from other states that are nominally unoccupied. The largest of these characters are (1) Sc d, (2) Pb p, and (3) Th p and d. The d-p hybridization between the B-site Sc ion and the surrounding O is common in this type of perovskite, as was emphasized previously,[5] while the Pb p character is the previously noted hybridization that is important for ferroelectricity in PZT. The hybridization on the Th site involves nominally unoccupied p states as in Pb (with similar strength as measured by the p character inside atomic spheres, although Th has no s lone pair), and an additional d component, which is absent on Pb.

Comparison of the panels of Fig. 1 shows a substantial change in the band gap upon structural relaxation. Since this gap is between an O p derived valence-band and a Th $5f$ conduction-band edge, one might suppose that this reflects hybridization between Th f states and O p states. Relative to the valence-band edge, the center of the Th $5f$ density of states shifts by ~ 2 eV in going from the ideal cubic perovskite to the relaxed lowest-energy monoclinic structure. Chemical effects involving the f states of light actinides are known,[32–34] but here this is not the case. Instead the shift is almost all due to on-site effects, in particular a change in the Coulomb potential at the Th site as it moves in its O cage. This is shown by the fact that there is a similar sized relative shift of the Th $1s$ core level with respect to the $1s$ of the O ions towards which it moves, while certainly these core levels are not involved in any bonding. Table I gives the cation $1s$ core-level shifts relative to the average O $1s$ position and the highest energy O $1s$ position.[35] The ~ 2.3 eV shift of the Th $1s$ level relative to the highest O $1s$ is remarkably close to the shift of the Th $5f$ level with respect to the valence-band edge. The signs of the $1s$ shifts show that the Th moves to a more favorable (for its Coulomb energy) position for a cation and the Sc to a less favorable position for a cation. This is one indication that the Th is driving the distortions and the Sc is responding.

In general, such shifts in the on-site Madelung potential should be considered when relating changes in band struc-

TABLE I. Energy shift, in eV, of the cation 1*s* levels in $ThPbSc_2O_6$ for different symmetry relaxations. The energies are relative to the O 1*s* position and the shifts are the energy in the relaxed structures relative to the ideal cubic perovskite. Two numbers are given: the shift relative to the average O 1*s* level (av), and relative to the highest O 1*s* (max).

	TET(av)	TET(max)	C_m(av)	C_m(max)
Th	1.96	1.65	2.63	2.34
Pb	0.22	−0.10	0.43	0.14
Sc(1)	−0.54	−0.85	−1.23	−1.52
Sc(2)	−0.54	−0.85	−1.17	−1.46

TABLE II. Energetics of lattice distortions in some perovskite scandates. The energies are in mRy per Sc, for various symmetry constrained structures (see text). All calculations are at the calculated LDA equilibrium volume for the undistorted cubic perovskite, except for (Th,Ba)ScO_3, which was studied under compression at the volume of (Th,Pb)ScO_3.

	E_{RHO}	E_{TET}	E_{R111}	E_{R001}	E_{R3}	E_{C_m}
$YScO_3$	−49	−80	−140	−109		
$BiScO_3$	−82	−73	−87	−74		
(Th,Pb)ScO_3	−41	−49	−65	−58	−67	−88
(Th,Ba)ScO_3	−35	−44	−44	−35		−78

ture with lattice distortion to changes in hybridization, especially in materials like these where there is a large misfit and as a result large atomic displacements. The conclusion that there is only a small amount of hybridization of the Th *f* levels is also consistent with the fact that there is very little Th *f* character in the occupied valence bands.

IV. LATTICE INSTABILITIES

As mentioned, the tolerance factor *t* plays a major role in determining the patterns of lattice instabilities in perovskites. The tolerance factors of the materials considered here are 0.91, 0.90, and 0.81 for $Th_{0.5}Pb_{0.5}ScO_3$ (averaged), $BiScO_3$, and $YScO_3$, respectively. This places $BiScO_3$ on the borderline of the region of perovskite stability and $YScO_3$ well outside it, while (Th,Pb)ScO_3 is also borderline but may be perovskite. In fact, $BiScO_3$ is known from experiment to crystallize in a nonperovskite structure under normal conditions, but the alloy of it with $PbTiO_3$ has a large range of perovskite stability,[13] and in fact a triclinic distorted perovskite modification of $BiScO_3$ as reported via high-pressure synthesis.[36,37] There is an additional factor to consider in (Th,Pb)ScO_3. The size of Th^{4+} is smaller than Pb^{2+}, and the high Th^{4+} valence will increase the strength of Coulomb interactions involving it. This may be expected to provide a strong *local* driving force for structural distortions around the Th sites.

To understand the basic patterns of the lattice distortions and the trends in the ferroelectric instability, we first consider these types of instability separately. LDA calculations were done at the equilibrium cubic volume separately for octahedral rotation around [111] and [001], as well as ferroelectric rhombohedral and tetragonal states. These were done by imposing space-group symmetries that allow the desired mode (centrosymmetric with 10 atom cells for the rotations and noncentrosymmetric with primitive cells for the ferroelectric distortions). In the primitive perovskite cell, the octahedral rotation is a pure mode at the *R* point (R_{25}), while the ferroelectric mode is part of a manifold of transverse optic modes. For the octahedral rotation, we calculated the energetics of the lattice distortions corresponding to this mode in all three materials, around two axes ([001] and [111]). For the ferroelectric mode, we fully relaxed the atomic positions within the unit cell, choosing symmetries that allow the ferroelectric displacements, but not rotation of the octahedra. In all cases, except the tetragonal ferroelectric, the lattice parameters were held at their cubic values. For the tetragonal ferroelectric state, the c/a ratio was varied, keeping the cell volume constant.

Considering the tolerance factors, it may be expected that octahedral rotation figures prominently in the lattice instabilities. This is clearly seen in the energetics. These are given in Table II, which lists the energies relative to the undistorted cubic structure of the constrained rhombohedral ferroelectrics (RHO), tetragonal ferroelectric (TET), octahedrally rotated around [111] (*R*111), and octahedrally rotated around [001] (*R*001) structures, as well as two complex structures, discussed below. Results for a (Th,Ba)ScO_3 supercell compressed to the volume of the (Th,Pb)ScO_3 cell are also given. This calculation was done to help understand the roles of Th and Pb.

In all cases, rotation about [111] leads to a lower energy than rotation around [001], presumably because in the latter case, not all the O atoms move towards an *A*-site ion. The extremely small tolerance factor of $YScO_3$ leads to a deep well for the *R*111 distortion of 140 mRy/Sc, which considering the large rotation and the fact that all other coordinates were held fixed in the calculation of the energetics of the rotational mode, is no doubt an underestimate, and in any case the true ground state would not be distorted perovskite. Varying the lattice parameter in a 5% range did not change the rotational energetics significantly. This is in contrast to the situation in Pb(Zr,Ti)O_3, presumably because of the much larger rotational instability in $YScO_3$ and the relative softness of ScO_6 octahedra compared with TiO_6. The rotational instabilities of the other compounds are smaller, following the trend in the tolerance factors.

The energy scale of the ferroelectric phases in $YScO_3$ is much lower, but still substantial. The RHO and TET states are nearly degenerate as long as tetragonal strain relaxation (i.e., c/a different from unity) is not allowed. Interestingly, as shown in Fig. 2, the energy of the relaxed TET state as a function of the strain has its minimum at a very large c/a ~ 1.3. This is related to the small *A*-site cation, which allows the formation of a layered structure with a compressed in-plane lattice constant. This compression brings the oxygens closer to the *A*-site ion. As mentioned, the rotational instability is driven by the size mismatch between the *A*- and *B*-site cations. A small *A*-site cation also gives a ferroelectric instability, as seen in $YScO_3$, but of smaller size than the rota-

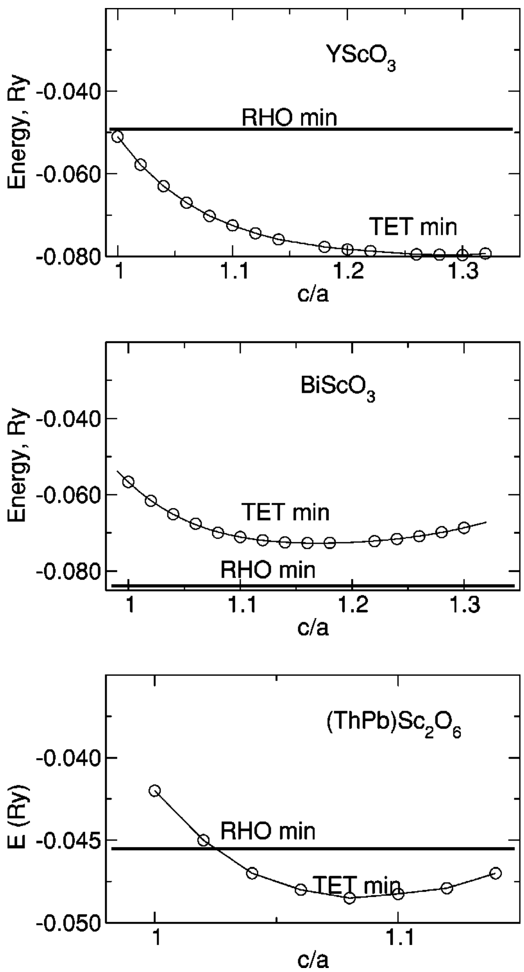

FIG. 2. Energy as a function of tetragonal strain c/a, $YScO_3$, $BiScO_3$, and $(Th_{0.5},Pb_{0.5})ScO_3$. The solid bottom line stands for the rhombohedral ferroelectric state. All atomic positions are fully relaxed consistent with the ferroelectric symmetry. Energies are per Sc.

tional instability. However, there is an additional factor, i.e., covalency between the *A*-site cation and the surrounding O that can tip the balance.[5] Thus the energetics of the ferroelectric states do not follow the trend in tolerance factors. Instead, $BiScO_3$ shows a deep ferroelectric minimum, with the RHO ferroelectric state strongly favored over the tetragonal. If constrained to be tetragonal ferroelectric, $BiScO_3$ would also have a large c/a ratio, as shown in Fig. 2 and as noted by Iniguez and co-workers.[15] In $(Th,Pb)ScO_3$, the TET state is slightly favored over the RHO state, but neither ferroelectric instability is as strong as the rotational instabilities. However, like the other two materials, a large tetragonality (here $c/a=1.08$) is predicted.[38] Unlike $YScO_3$ the ferroelectric instabilities are reasonably close in energy to the rotational instability, raising the question of whether they may coexist. In fact they do, as discussed in the following section.

The differences between $YScO_3$ and $BiScO_3$ can be related, at least qualitatively, to the differences in the electronic structure, in particular, the different angular character of the Y- and Bi-centered bonding orbitals. The Y ions are very small and contribute mostly unoccupied states of *d* character, and are thus only weakly hybridized with the valence states of primarily oxygen *p* character. Because of this the energetics are not very sensitive to the bond directions around Y. This is also reflected in the 2 eV dielectric gap present in the electronic structure of $YScO_3$.

There is a significant difference in the energetics without tetragonal strain (keeping cubic lattice vectors): with Y on the *A* site, the RHO and TET energies are very close, whereas the RHO state is strongly favored over the TET state in the Bi compound [cf. Fig. 2] and to a lesser extent in $(Th,Pb)ScO_3$.

This is remarkable because, starting from the undistorted ideal perovskite structure, the ferroelectric instability is isotropic, so that for very small displacements the RHO and TET energies are the same. Furthermore, the ferroelectricity is driven by the *A*-site ion, which is in a 12-fold coordinated site, and therefore is at first sight in an isotropic environment. The explanation is that the *A*-site cation behaves as if it has more room for motion along [111] relative to [001]. This is not due to its nearest-neighbor local environment but because of the interaction with the ScO_6 octahedra. In particular, the octahedra are strongly covalent and polarizable. This is seen in the shifts of Sc relative to O in the ferroelectric modes. Since the ferroelectric instability is driven by the Coulomb interaction, the polarizability of the ScO_6 octahedra is important to its energetics (cf. Clausius-Mossotti). This polarizability is also isotropic for small distortions. However, this is limited by the hard-core ionic repulsion between Sc and the neighboring O.

In the simplest picture, where the ScO_6 polarizability is large and therefore plays the dominant role in the energetics, and where the polarizability is constant until the hard ionic overlap is reached and then becomes small for larger ScO_6 distortions, the *A*-site cation would behave as if it has $\sqrt{3}$ more room to move in the [111] direction than the [100]. This is due to the geometric constraints on the Sc motion in the oxygen octahedra. The difference between $YScO_3$ and $BiScO_3$ may then be due to the fact that the smaller lattice parameter in the former compound compresses the ScO_6 octahedra so that its polarizability plays a smaller role. Then the isotropic nature of the dominant *A*-site motion underlying the ferroelectric instability is reflected in the small difference between the rhombohedral and unstrained $(c/a=1)$ tetragonal ferroelectric energies. This, however, is only one factor. Cation-cation repulsion, either directly or via O bond saturation, as discussed by Grinberg and co-workers,[39] may also be important.

A similar stabilization of the RHO ferroelectric state relative to the constrained pseudocubic TET configuration is seen in titanates, such as $PbTiO_3$, but with a considerably smaller energy difference.[5] This may be because the TiO_6 octahedra are stiffer than the present ScO_6 and so the anisotropy of their higher-order polarizability is less important. This qualitative explanation would be consistent with the crossover from TET to RHO instabilities in $Pb(Zr,Ti)O_3$ as the Zr concentration is increased through the MPB, since the larger, $4d\,ZrO_6$ octahedra would be expected to be more polarizable than the TiO_6 octahedra. This picture is also consistent with local structures in large supercells[39] as well as

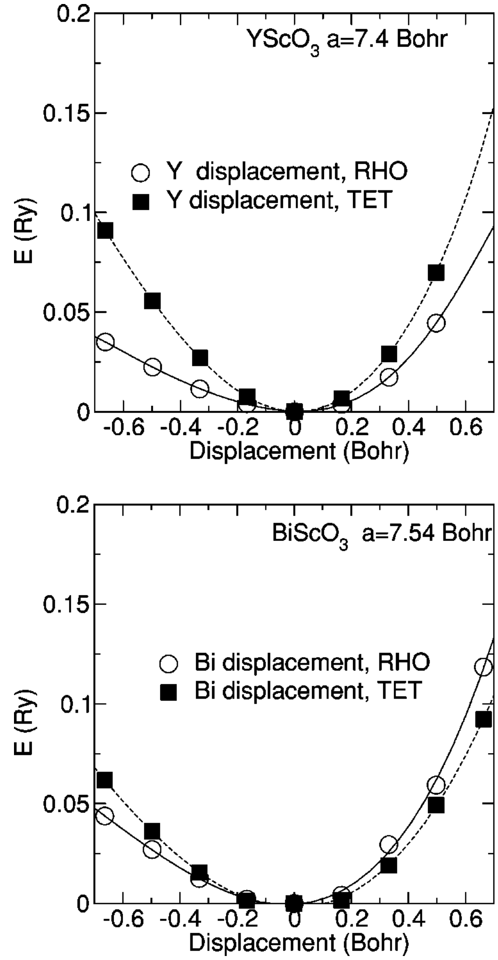

FIG. 3. Energy per single Sc unit as a function of the displacement of A-site ion from the equilibrium position in $YScO_3$ (left) and $BiScO_3$ (right) for both RHO (open circle) and TET (filled square) distortions. The energy zero for is set to the equilibrium energy, so the zeros are different for the two curves in each panel.

structural observations in $PbSc_{1/2}Nb_{1/2}O_3$-$PbTiO_3$ alloys.[40]

Bismuth ions on A sites donate p electrons into hybridized orbitals with mixed Bi p and O p character. The 0.3 eV LDA band gap is between Bi and O derived states. The low-lying Bi p bands and their strong hybridization with the occupied O p bands (note that the unoccupied Bi p orbitals are quite extended and therefore will have a large overlap with the O p's) constitutes the band-structure description of the so-called polarizable lone pair. This favors ferroelectric distortions relative to octahedral rotation. This is shown in Fig. 3, where the energy is plotted as a function of A-site ion only displacement around RHO and TET equilibria while holding all other ions fixed. The larger Bi ions with stronger coupling to oxygens make the crystal more resistant against the tetragonal strain, while Bi-O covalency softens the ferroelectric distortion.

The ferroelectric distortions in all these materials consist of shifts of the cations relative to the surrounding oxygens. As expected, the main displacements are of the A-site ions, but sizable shifts of the Sc ions also occur, reflecting the nonrigidity of the ScO_6 octahedra. This in turn is related to

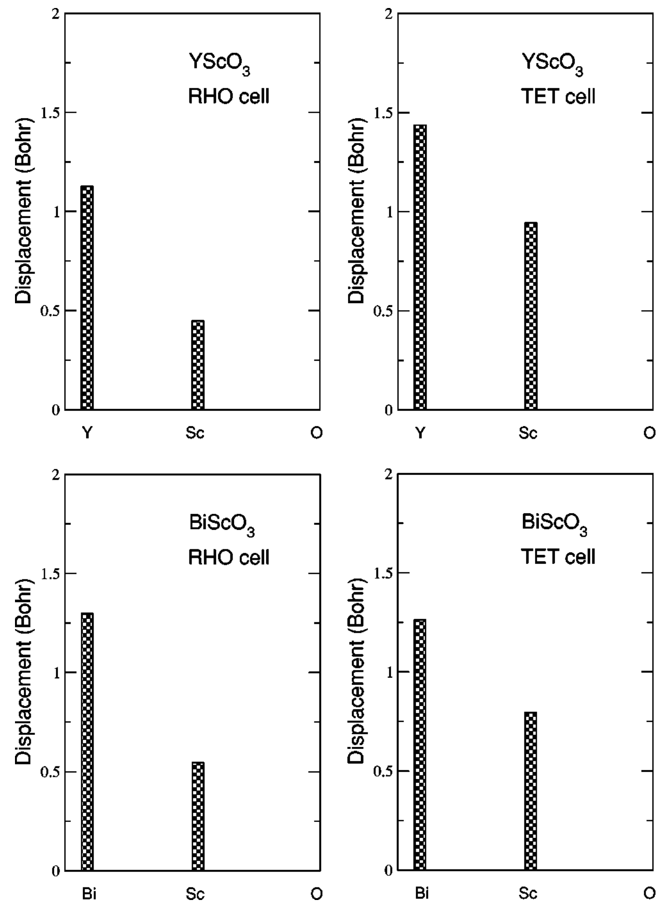

FIG. 4. Displacement diagram for RHO (left) and TET (right) distortions in $YScO_3$ (top) and $BiScO_3$ (bottom). The plots give the displacements of the A- and B-site cations in the relaxed structures relative to the O center of mass.

the larger size of Sc^{3+} relative to Ti^{4+}, which reduces O-O interactions, and covalency between Sc and O, as seen in the electron structure and as noted previously for $BiScO_3$ by Iniguez and co-workers.[15] This is shown in Fig. 4 for $YScO_3$ and $BiScO_3$. Similar observations have been made for $PbZrO_3$.[41] This pattern is also present in $(Th,Pb)ScO_3$ as shown in Fig. 7. In particular, the distortions for the constrained TET and RHO states consist primarily of a shift of the A-site cations with respect to the O center of mass, with smaller but still sizable shifts of the Sc in the same direction. Interestingly, the largest displacement is that of the small Th ion, which because of this large displacement and its high nominal charge would be significant for the polarization.

In solid solutions, such as $Pb(Zr,Ti)O_3$ (PZT) and $Pb(Mg,Nb,Ti)O_3$ (PMN-PT), the lattice parameter increases moving across the phase diagram from the $PbTiO_3$ end point. As a result the tolerance factor decreases, the volume available to the Pb A site increases, and the magnitude of the ferroelectric instability also increases. However, the ferroelectric Curie temperature T_C decreases. This can be understood in terms of phase-space arguments. In particular, as the lattice expands, other instabilities, in particular other off-centering patterns (e.g., non-Γ-point off-centering) as well as the rotational instabilities also become stronger, providing

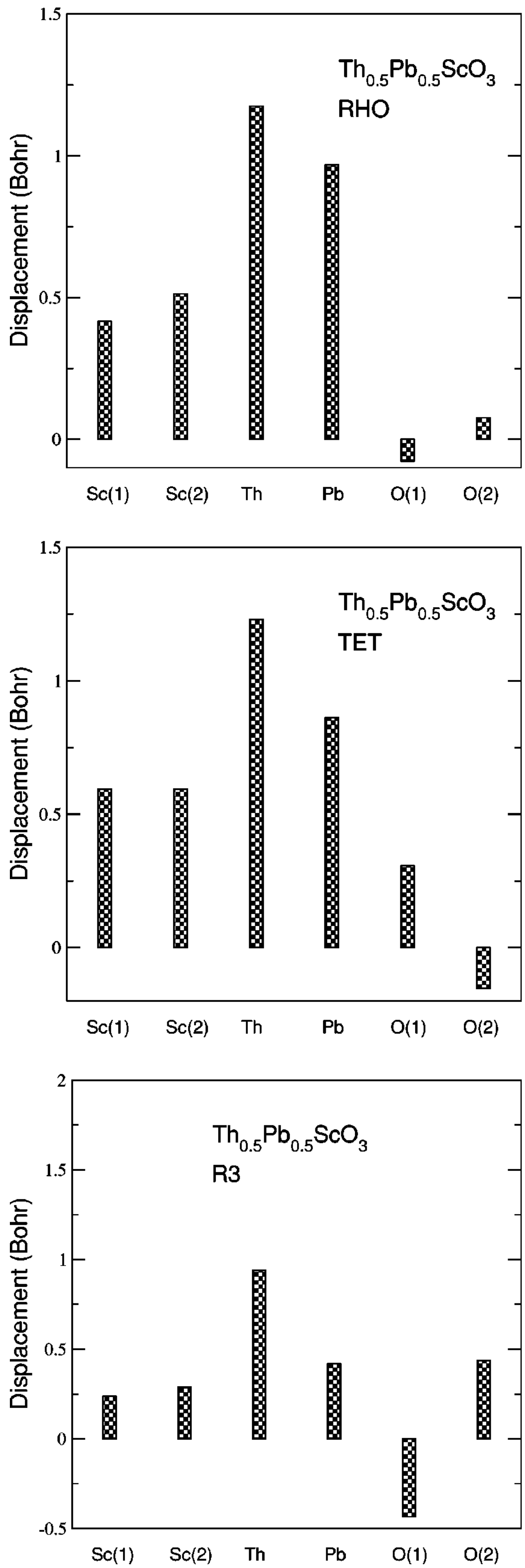

FIG. 5. (Color online) The $R3$ structure. The figure shows the ideal perovskite positions as spheres, with the displacements to the $R3$ structure given by vectors. This structure consists of coexisting ferroelectricity and [111] rotations of the octahedra.

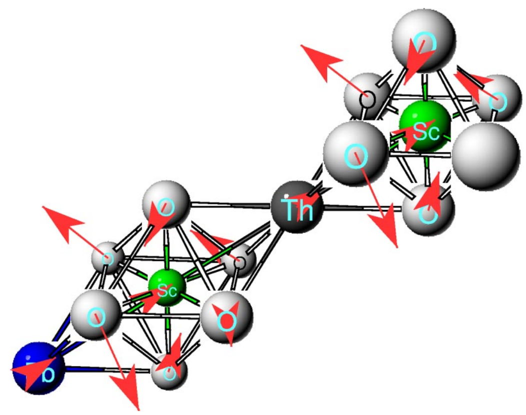

FIG. 6. Ferroelectric displacements in $Th_{0.5}Pb_{0.5}ScO_3$ supercells, in the relaxed rhombohedral ferroelectric state, not allowing rotation (top), in the tetragonal ferroelectric state, also without rotation (middle) and relaxed in the trigonal $R3$ symmetry allowing coexistence of ferroelectricity and rotation of the ScO_6 octahedra about [111] (bottom).

more phase space for fluctuations and depressing T_C. In fact, effective Hamiltonian simulations neglecting the rotational instabilities of PZT substantially overestimate T_C.[8]

Recently, Eitel and co-workers have proposed the use of alloys of $PbTiO_3$ with low tolerance factor materials to obtain higher T_C at the MPB, and have demonstrated the success of this approach in $BiScO_3$-$PbTiO_3$ alloys.[13,14] We propose that the large difference in energy between the TET and RHO ferroelectric states in $BiScO_3$ and the very large energy scale of the RHO state (related to the strong Bi-O covalency, strongly favoring ferroelectricity) are responsible for the high T_C at the MPB in $BiScO_3$-$PbTiO_3$ rather than the low tolerance factor of $BiScO_3$. In particular, these two ingredients put the MPB close to the $PbTiO_3$ end point, where rotations are less important and T_C is higher.

The effects of partial A-site substitutions in these materials can be expected to be quite different for rotational and ferroelectric distortions. In particular, because of the shared oxygen ions connecting the perovskite octahedra, rotations of nearby octahedra must be at least short-range correlated. However, off-centerings of cations on different sites can be relatively independent. This is reflected, for example, in the relatively weak dispersion of the ferroelectric mode away from the Γ point in Pb based ferroelectrics compared with the much stronger upward dispersion of rotational (e.g., R_{25}) modes moving away from the zone boundary.[42] Thus substitution of a larger ion on some of the A sites would be expected to have a stronger effect on the rotational instability than on the ferroelectric instability. This would be clearest if the octahedra were very rigid, but some effect ought to be present in these scandates as well. To check this we repeated the calculations for (Th,Pb)ScO_3 with (Th,Ba)ScO_3 compressed to the volume of (Th,Pb)ScO_3. Besides confirming this expectation, the calculation allows us to understand the role of Pb covalency in driving the ferroelectric instability in this material. As shown by the energetics in Table II, the substitution of larger ions does indeed reduce the rotational instabilities, while having only a small effect on the ferro-

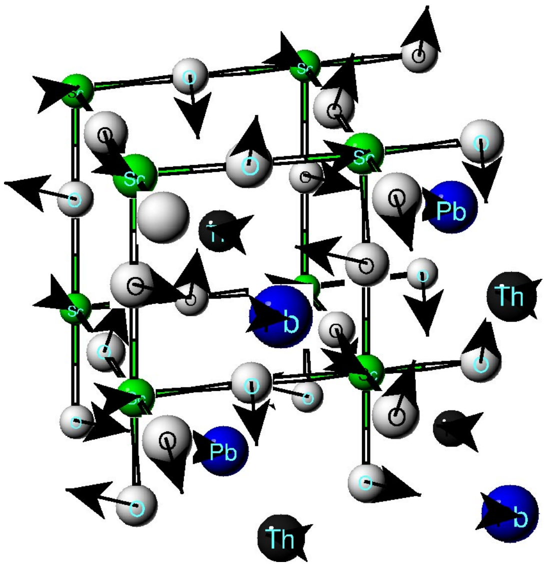

FIG. 7. (Color online) The fully relaxed C_m structure of a $Th_{0.5}Pb_{0.5}ScO_3$ supercell (see text). The displacements from the ideal cubic perovskite positions with respect to the center of mass are shown as vectors for each atom. The lines are the Sc-O bonds.

electric instabilities. This supports the view that the small Th *A*-site ion is the main driver of the ferroelectricity in this material.

V. COEXISTENCE OF ROTATIONAL AND FERROELECTRIC DISTORTIONS

The rotational instabilities and the ferroelectric instabilities in $(Th,Pb)ScO_3$ are both consequences of the low tolerance factor, $t \ll 1$, which leads to an overly large A site–O distance. Since the driving force for these instabilities is the same, one may expect them to be antagonistic. However, when viewed as distortions of the cubic perovskite structure, one notes that they belong to different symmetries and therefore are independent in lowest order, suggesting coexistence. To examine this issue, and come closer to the ground state, we did two additional calculations. First of all we relaxed the structure in a trigonal $R3$ symmetry. This allows rotation of the octahedra around [111] and the ferroelectric RHO type of distortion (it is a subgroup of $R3c$, which was used for the $R111$ calculations and of $R32$, which was used for the RHO distortion). This calculation was done using the cubic lattice vectors (i.e., not allowing any rhombohedral strain, which in perovskites tends to be small). The relaxed structure (Fig. 5) included both a substantial RHO type ferroelectric distortion and rotations. We denote this structure as $R3$ in the following. The $R3$ energy is 67 mRy/Sc below the cubic perovskite. This is, however, only 2 mRy/Sc below the $R111$ rotated structure. As shown in the bottom panel of Fig. 6, the displacement pattern for the relaxed structure shows a large Th displacement, roughly 3/4 as large as in the pure RHO structure, but considerably reduced Pb displacement. This presumably results from the difference in ionic radii—all octahedra in this supercell rotate by the same amount, this leaves ample room for Th to off-center but not for Pb.

TABLE III. Atomic positions in the relaxed C_m $Pb_{0.5}Th_{0.5}ScO_3$ supercell at $c/a=1$ in lattice coordinates. For reference the positions of the atoms in the ideal cubic perovskite structure (denoted c) are also given. The lattice vectors are $(a,a,0)$, $(a,-a,0)$, and $(a,0,a)$. O(3) and O(4) are related by symmetry, as are O(5) and O(6).

	x_1	x_2	x_3	$x_1(c)$	$x_2(c)$	$x_3(c)$
Sc(1)	0.252	0.751	0.499	0.25	0.75	0.50
Sc(2)	0.748	0.248	0.505	0.75	0.25	0.50
Th	0.529	0.500	−0.001	0.50	0.50	0.00
Pb	−0.002	−0.002	0.004	0.00	0.00	0.00
O(1)	0.416	0.000	0.000	0.50	0.00	0.00
O(2)	0.126	0.499	0.002	0.00	0.50	0.00
O(3)	−0.076	−0.076	0.621	0.00	0.00	0.50
O(4)	−0.076	0.455	0.621	0.00	0.50	0.50
O(5)	0.547	0.546	0.378	0.50	0.50	0.50
O(6)	0.547	0.076	0.378	0.50	0.00	0.50

Calculations were also done for the supercell without symmetry constraints using cubic and tetragonal lattice vectors. The final relaxed structures for this supercell were monoclinic C_m and strongly rotational in character (the main rotation is by around $[1\bar{1}0]$, by an average 17°). The monoclinic mirror plane is the only remaining symmetry. It also has weak co-existing ferroelectricity and distorted octahedra, as shown in Fig. 7. The atomic positions are given in Table III. The energy of this structure for the present $(Th,Pb)ScO_3$ supercell is 88 mRy below the ideal cubic perovskite and 21 mRy below the $R3$ structure. The energy as a function of c/a is minimum at the pseudocubic value $c/a=1$. The relatively weak ferroelectricity in this cell still involves off-centering of the Th with respect to the surrounding O by a substantial $0.33a_0$ (along [110], i.e., normal to the primary rotation axis). However, it cannot be said from the present calculations whether a larger more realistic supercell would be ferroelectric. The pattern in this supercell is related to the specific (Th,Pb) ordering. This suggests that the ferroelectric ordering of Th displacements may be an artifact of the simple supercell considered here. Interestingly, a similar low-energy monoclinic structure is found for the $(Th,Ba)ScO_3$ supercell. The reason that this structure is low in energy is apparently that the distortion of the octahedra allows the O atoms that rotate towards the Th to move a large distance and those moving towards the Pb (or Ba) to move less. This softness of the octahedra and the resulting relative ineffectiveness of Ba to suppress the formation of rotated phases is specific to these scandates. Such a result would not be expected in titanates.

In any case, the qualitative picture of $Th_{0.5}Pb_{0.5}ScO_3$ as having primarily rotational lattice instabilities, with nearby but higher in energy ferroelectric states remains. Based on these results, we do not think that $Th_{0.5}Pb_{0.5}ScO_3$ would be a good ferroelectric, assuming that it can be made in perovskite structure at all. However, it is worthwhile to speculate whether it could be useful to alloy it with other materials to make new piezoelectric compositions. We discuss the trends and speculate about possible new materials in the next section.

VI. SUMMARY AND DISCUSSION

Structural relaxations for small supercells of $Th_{0.5}Pb_{0.5}ScO_3$, $BiScO_3$, $YScO_3$, and compressed $Th_{0.5}Ba_{0.5}ScO_3$ were done. Because of the small size of these supercells and the assumed ordering of the *A*-site cations the results should not be interpreted as predictions of ground states for these materials. Instead they should be viewed as simplified situations that help in understanding the trends in the lattice instabilities of these scandates. The trends that emerge from our calculations are as follows.

(1) Th is tetravalent on the perovskite *A* site, as expected, and has weak but not negligible hybridization with O.

(2) The small *A*-site ions in these materials favor rotational instabilities, in accord with the tolerance factor.

(3) They also favor ferroelectric instabilities, but the magnitude of these is small in the absence of covalency.

(4) If rotations are suppressed, $Th_{0.5}Pb_{0.5}ScO_3$ would favor a tetragonal ferroelectric state.

(5) The ScO_6 octahedra are softer than the TiO_6 octahedra in materials like $Pb(Zr,Ti)O_3$, this complicates using partial substitution of large cations to suppress the rotations, and also reduces the volume dependence of the rotational instabilities.

(6) The small *A*-site ions lead to smaller lattice parameters and also larger tetragonality in the tetragonal ferroelectric state, both of which, all other things being equal, are desirable in piezoelectrics.

The results imply that ferroelectric states can be obtained in materials based on $(Th,Pb)ScO_3$ by suppressing rotations of the ScO_6 octahedra. This might be done by replacing some of the *A*-site ions with larger species and by alloying the *B* site with Ti or other smaller ions to make octahedra more rigid. Considering the energetics without rotations, one possibility would seem to be alloying $BiScO_3$ with $(Th,Pb)ScO_3$. The motivation is that the (Th,Pb) substitution for Bi would favor a tetragonal ferroelectric state, and perhaps lead to an MPB. Based on the calculated energetics, particularly the very strong energy separation of the RHO and TET states in $BiScO_3$, relative to $(Th,Pb)ScO_3$, the MPB, if it exists, would likely be in the Th rich side of the pseudobinary phase diagram. The second possibility would be to investigate alloying $PbTiO_3$ or PZT with $(Th,Pb)ScO_3$. The small Th *A*-site ions may then favor increased tetragonality, which would be favorable, albeit at the expense of further bringing in the rotational modes and therefore lowering T_C.

ACKNOWLEDGMENTS

The authors are grateful to L. L. Boyer, R. E. Cohen, P. K. Davies, J. Iniguez, A. M. Rappe, and U. V. Waghmare for helpful discussions. We particularly thank P. K. Davies for helpful suggestions. This work is supported by the Office of Naval Research, the Center for Piezoelectrics by Design and DoD HPCMO computer access. Some calculations were performed with the DoD-AE code.

[1] M. E. Lines and A. M. Glass, *Principles and Applications of Ferroelectrics and Related Materials* (Clarendon, Oxford, 1977).
[2] B. Jaffe, W. R. J. Cook, and H. Jaffe, *Piezoelectric Ceramics* (Academic Press, New York, 1971).
[3] K. Uchino, *Piezoelectric Actuators and Ultrasonic Motors* (Kluwer Academic Press, Boston, 1996).
[4] R.E. Cohen and H. Krakauer, Phys. Rev. B **42**, 6416 (1990).
[5] R.E. Cohen, Nature (London) **358**, 136 (1992).
[6] S.-E. Park and T.R. Shrout, J. Appl. Phys. **82**, 1804 (1997).
[7] H. Fu and R.E. Cohen, Nature (London) **281**, 403 (2000).
[8] L. Bellaiche, A. Garcia, and D. Vanderbilt, Phys. Rev. Lett. **84**, 5427 (2000).
[9] B. Noheda, D.E. Cox, G. Shirane, L.E. Cross, and S.-E. Park, Appl. Phys. Lett. **74**, 2059 (1999).
[10] R. Guo, L.E. Cross, S.-E. Park, B. Noheda, D.E. Cox, and G. Shirane, Phys. Rev. Lett. **84**, 5423 (2000).
[11] B. Noheda, D.E. Cox, G. Shirane, S.E. Park, L.E. Cross, and Z. Zhong, Phys. Rev. Lett. **86**, 3891 (2001).
[12] See, for example, the papers in *Fundamental Physics of Ferroelectrics*, edited by P.K. Davies and D.J. Singh, AIP Conf. Proc. No. 677 (AIP, Melville, NY, 2003).
[13] R.E. Eitel, C.A. Randall, T.R. Shrout, P.W. Rehrig, W. Hackenberger, and S.-E. Park, Jpn. J. Appl. Phys., Part 1 **40**, 5999 (2001).
[14] R.E. Eitel, C.A. Randall, T.R. Shrout, and S.-E. Park, Jpn. J. Appl. Phys., Part 1 **41**, 2099 (2002).
[15] J. Iniguez, D. Vanderbilt, and L. Bellaiche, Phys. Rev. B **67**, 224107 (2003).
[16] G. Saghi-Szabo, R.E. Cohen, and H. Krakauer, Phys. Rev. B **59**, 12 771 (1999).
[17] N.J. Ramer and A.M. Rappe, Phys. Rev. B **62**, 743 (2000).
[18] M. Fornari and D.J. Singh, Phys. Rev. B **63**, 092101 (2001).
[19] Z. Wu and H. Krakauer, Phys. Rev. B **68**, 014112 (2003).
[20] B.G. Hyde and S. Andersson, *Inorganic Crystal Structures* (Wiley, New York, 1988).
[21] O. Muller and R. Roy, *The Major Ternary Structural Families* (Springer-Verlag, New York, 1974), p. 221.
[22] S.V. Halilov, M. Fornari, and D.J. Singh, Appl. Phys. Lett. **81**, 3443 (2002).
[23] I. Grinberg and A. M. Rappe, in *Fundamental Physics and Ferroelectrics* (Ref. 12), p. 130.
[24] D.Y. Suáres-Sandoval and P.K. Davies, Appl. Phys. Lett. **82**, 3215 (2003).
[25] M. Labeau, I.E. Grey, J. C Joubert, J. Chenevas, A. Collomb, and J.C. Guitel, Acta Crystallogr., Sect. B: Struct. Sci. **41**, 33 (1985).
[26] T. Yoshimura and S. Trolier-McKinstry, Appl. Phys. Lett. **81**, 2065 (2002).
[27] D. J. Singh, *Planewaves, Pseudopotentials and the LAPW Method*

(Kluwer Academic, Boston, 1994).

[28] D. Singh, Phys. Rev. B **43**, 6388 (1991).

[29] M.D. Jones, J.C. Boettger, R.C. Albers, and D.J. Singh, Phys. Rev. B **61**, 4644 (2000).

[30] J. Kunes, P. Novak, R. Schmid, P. Blaha, and K. Schwarz, Phys. Rev. B **64**, 153102 (2001).

[31] S.V. Halilov and D.J. Singh, Phys. Rev. B **67**, 012501 (2003).

[32] J. Friedel, J. Phys. Chem. Solids **1**, 175 (1956).

[33] M.S.S. Brooks, B. Johansson, and H.L. Skriver, in *Handbook on the Physics and Chemistry of the Actinides*, edited by A.J. Freeman and G. Lander (Elsevier, Amsterdam, 1984), Vol. 1, Chap. 3.

[34] B. Johansson, Hyperfine Interact. **128**, 41 (2000).

[35] As the octahedra rotate towards the ground-state structure the O $2p$–Sc $3d$ linear chains are bent, reducing the $pd\sigma$ hopping, while at the same time the O on-site energies are shifted, so that the top of the valence band, from which the Th $5f$ positions was measured, is mostly from the O with the highest on-site energy. This is the O_{ap} as defined in the caption of Fig. 1 for the monoclinic structure.

[36] Y.Y. Tomashpolski and Y.N. Venettsev, Izv. Akad. Nauk SSSR, Neorg. Mater. **5**, 1279 (1969) [Inorg. Mater. **5**, 1087 (1969)].

[37] Y. Inaguma, A. Miyaguchi, M. Yoshida, T. Katsumata, Y. Shimojo, R. Wang, and T. Sekiya, J. Appl. Phys. **95**, 231 (2004).

[38] Since our calculations are at the LDA volume, which is almost certainly an underestimate, we probably underestimate the tetragonal c/a as well. The volume dependence of tetragonality in $PbTiO_3$ was discussed in detail in Ref. 43.

[39] I. Grinberg, V.R. Cooper, and A.M. Rappe, Nature (London) **419**, 909 (2002).

[40] R. Haumont, B. Dkhil, J.M. Kiat, A. Al-Barakaty, H. Dammak, and L. Bellaiche, Phys. Rev. B **68**, 014114 (2003).

[41] D.J. Singh, Phys. Rev. B **52**, 12 559 (1995).

[42] P. Ghosez, E. Cockayne, U.V. Waghmare, and K.M. Rabe, Phys. Rev. B **60**, 836 (1999).

[43] G. Saghi-Szabo, R.E. Cohen, and H. Krakauer, Phys. Rev. Lett. **80**, 4321 (1998).